



DOI: doi.org/10.21009/SPEKTRA.081.01

COMBINED METHOD OF BULK MATERIAL SHIELDING EVALUATION FOR 200 MEV HIGH ENERGY NEUTRON SOURCE USING PHITS MODELLING AND PARTIAL DENSITY

Fitrotun Aliyah^{1,2}, Azhar Abdul Rahman^{1,*}, Yasmin Md Radzi¹,
Imam Kambali³

¹*School of Physics, Universiti Sains Malaysia, Penang, Malaysia*

²*Department of Nuclear Engineering and Engineering Physics, Universitas Gadjah Mada, Yogyakarta, Indonesia*

³*Research Center for Accelerator Technology, National Research and Innovation Agency, Indonesia*

*Corresponding Author Email: arazhar@usm.my

Received: 26 January 2023

Revised: 13 April 2023

Accepted: 14 April 2023

Online: 28 April 2023

Published: 30 April 2023

SPEKTRA: Jurnal Fisika dan Aplikasinya

p-ISSN: 2541-3384

e-ISSN: 2541-3392



ABSTRACT

Neutron encounters difficulties in shielding protection. Thus, many researchers have performed simulation and experimental research on neutron shielding materials. The characteristic of materials is highly dependent on neutron energy. The evaluation of neutron shielding for various materials, such as iron, concrete, aluminum, and borated polyethylene (BPE), was conducted in this paper through simulation using a Monte Carlo code of PHITS 3.27 and calculation via partial density method. A mono-energetic neutron source with an energy of 200 MeV is emitted perpendicular to the shielding material with a thickness of 105 cm. The parameters measured in this analysis include flux, fast neutron removal cross-section, neutron depth dose, ambient dose $H^*(10)$ equivalent, and neutron dose reduction factor (RF). Results show that iron is a good material against high-energy neutron and secondary photon radiation at the energy range with the highest removal cross-section and the lowest RF value (0.39), followed by concrete, BPE, and aluminum. The integrated fluence and effective dose profiles were consistent with previous results in the literature. Benchmarking calculation of neutron dose RF was conducted with other publications and was in good agreement within the value range.

Keywords: shielding, monte carlo, neutron, radiation protection, partial density

INTRODUCTION

Neutrons are generated and used widely in the fission reactor industry and medical field. Secondary neutrons can be produced by interacting protons or heavy ion particles with target materials in accelerators. In addition to neutrons, the interaction of protons and heavy ions produces photons [1-6]. The utilization of heavy ions and protons in the health sector, such as cancer therapy, has rapidly progressed and continuously exponentially grown in the last decade. Particle Therapy Co-Operative Group (PTCOG) noted that as of April 2021, particle therapy had treated more than 290000 patients, of which 250000 patients using proton therapy, and the rest employed C-ion and He [7,8].

Neutron radiation is more harmful to human health than beta, gamma, and X-ray radiation because neutrons have a high linear energy transfer (LET) value [6,9]. Therefore, neutron radiation directly damages DNA cells by decreasing the oxygen enhancement ratio. Compared with low LET radiation, such as photons, repairing the damage caused by neutron radiation is difficult; the damage may also be less repairable [9]. Therefore, designing the shielding properly to withstand neutron radiation is necessary to create a safe environment for radiation workers and the general public.

Researchers have studied the material characteristics of neutron radiation for a long time, around the mid-1990s, since the introduction of neutron existence [10]. Safety and radiation protection aspects require important knowledge of the materials for neutron radiation shielding. In addition, the radiation shielding cost influences a significant portion of the entire cost of building facilities [11,12]. Shielding designers need material data, such as flux, mass attenuation or removal cross-section, effective dose, and reduction factor, during pre-construction.

Shielding calculations for neutron radiation are more complex than those for photons and beta radiation. The interaction between photons and materials is dominated by Compton scattering; however, photon shielding is mainly determined by material density. Neutrons, conversely, have different interaction properties in which density is a little but minor consideration. Neutrons can only interact with the nuclei of target atoms because they are neutral. The probability of atomic nucleus interactions highly depends on the primary neutron energy, the number, and the type of collisions it undergoes [13].

When the neutron energy is high, several phases are presented to stop the neutron: reducing the neutron energy to a thermal energy level below 0.025 eV (attenuation phase) and capturing thermalized neutrons (absorption phase). The fast neutron attenuation process generally results from a scattering phenomenon comprising elastic and inelastic scattering. Inelastic scattering occurs when neutrons collide with atomic nuclei and produce a compound nucleus, tailed by the release of low-energy neutrons and gamma rays. This interaction usually occurs when neutrons interact with heavy atomic nuclei. By contrast, elastic scattering usually occurs when a neutron collides with a low Z atomic nucleus by transferring kinetic energy [13].

A computational method with Monte Carlo code has proven that the simulation can accurately describe neutron interaction with matter. Japan Atomic Energy Agency (JAEA) has developed the Particle and Heavy Ion Transport code System (PHITS) for various purposes of nuclear

interaction analysis, including radiation shielding, radiation protection, accelerator design, cosmic rays, and medical application [1,14-20].

Research on shielding material properties for neutron radiation has been previously published [1,6,14], [21-25]. M. Fragopoulou and M. Zamani investigated and presented the calculation result of shielding neutron sources for various materials, including concrete, iron, polyethylene, and graphite, in several initial neutron energies from 1 eV to 100 MeV [12]. However, information on the shielding properties for a neutron energy of 200 MeV is lacking. A 200 MeV neutron is used in several facilities, such as the Los Alamos Neutron Science Centre (LANSCE), which built accelerator-coupled nuclear reactor systems incinerating actinides [26] and the accelerator beam at RCNP, Osaka University [27]. In addition, 200 MeV neutrons are produced as secondary radiation from proton and high-energy carbon ion therapy, which are currently operated in hospitals worldwide [7].

Vishwanath and Badiger also studied the effectiveness of some alloy materials for neutron and photon shielding but only in the 0.015 MeV to 15 MeV energy range [28]. The research results of Agosteo et al. provided shielding material data for various fast neutron energy comprising 200 MeV but limited for concrete and iron material and less comprehensive [29,30]. T. Koi et al. studied the attenuation of neutrons for the energy range between 100 and 400 MeV using an RCNP accelerator beam but limited to a thick carbon target [27]. A recent study from Stone et al. characterized some shielding materials for scattering neutrons for a maximum energy of 14 MeV [10]. Therefore, this study was conducted to meet the required data of shielding material properties from iron, concrete, Al, and BPE, especially for a fast neutron energy of 200 MeV. The data will be crucial in shielding design and pre-construction for selecting suitable high-energy neutron source shielding materials.

METHOD

The flux and effective dose of neutron radiation to the shielding material was calculated using the PHITS code. As illustrated in FIGURE 1, an initial geometry was developed to indicate the neutron source and shielding geometry arrangement in 2D dimensions. In this model, three material slabs with a thickness of 35 cm each (with a total thickness of 105 cm) are placed perpendicular to the direction of the neutron source, as illustrated in FIGURE 1. The red arrow shows the 2D planar beam of a mono-energetic neutron source of 200 MeV. The neutron source was assumed as a pencil beam, and the shielding was described as a cylinder slab with a close distance between the neutron source of around 0.01 cm.

The PHITS code simulates the transport of neutrons through the shielding media, such as iron, aluminum, concrete, and borated polyethylene (BPE), with various types of interactions along with the cross-section information in the JENDL-4.0 libraries data. TABLE 1 tabulates the data on shielding material properties, such as density and material composition. FIGURE 2 and 3 provide flux and neutron spectrum through the shielding material, respectively. The ambient dose $H^*(10)$ equivalent is measured at the point immediately behind the shielding. These data are obtained as output from (t-track) and (t-cross) tally, while the removal cross-section is calculated using the partial density method. The (t-track) calculation aims to visualize particle trajectories and calculate effective and ambient doses amongst the material,

while the (t-cross) tally aims to calculate particle fluence behind shielding. The Monte Carlo method is strongly influenced by historical numbers of particles [17], [31-34]. Therefore, 10^6 history numbers were used in the current study to reduce uncertainty errors. The relative error of flux, ambient dose equivalent, and effective dose rate were maintained below 5% [35]. Benchmarking is conducted with simulation and experimental data from other publications to validate the simulation results.

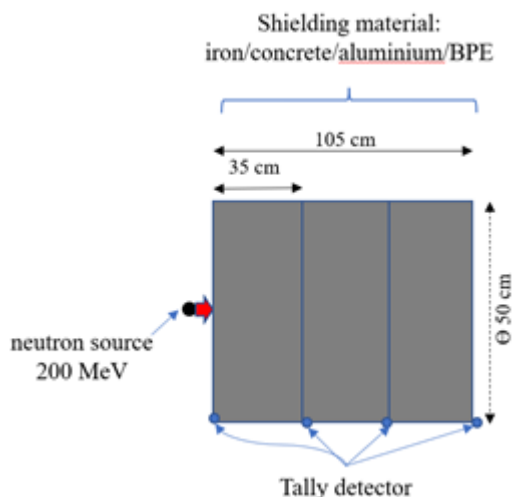


FIGURE 1. Conceptual geometry (2D) for neutron source and shielding material

Removal cross-section for fast neutron

The effectiveness of neutron shielding materials can be defined from the fast neutron removal cross-section value (Σ_R). A removal cross-section is utilized for estimating the fast neutron attenuation. It is defined as the chance of a fast neutron or the interaction of neutron fission-energy level, which separates it from penetrating the non-collided neutron group [36-38].

The removal cross-section (Σ_R) is part of the total macroscopic cross-section (Σ_t), which is a quantity that shows the neutron probability of colliding with an atomic nucleus. The collision depends on the nuclei number and the microscopic cross-section value. By contrast, the total microscopic cross-section (σ_t) is the probability of neutron interaction at the energy range colliding with the atomic nucleus, comprising scattering and absorption interactions [38]. The following equations show the relationship between the total microscopic cross-section (σ_t), the total macroscopic cross-section (Σ_t), and the removal cross-section (Σ_R).

$$\sigma_t = \sigma_s + \sigma_a \quad (1)$$

$$\Sigma_t = \frac{\rho N_A \sigma_t}{A} \quad (2)$$

When neutron traversed the material with high hydrogen content, for energy 2 and 12 MeV, the value was almost constant. By contrast, when a neutron passed a material with a low hydrogen fraction, $\Sigma_R = \frac{2}{3} \Sigma_t$ for the energy of 6–8 MeV [39-41]. The macroscopic removal cross-section of a compound material comprising numerous elements is identified via summation of all components [38,41]:

$$\Sigma_{R, compound} = \left(\frac{\Sigma_R}{\rho}\right)_1 W_1 + \left(\frac{\Sigma_R}{\rho}\right)_2 W_2 + \left(\frac{\Sigma_R}{\rho}\right)_3 W_3 + \dots \quad (3)$$

$$\Sigma_{R, compound} = \sum_i W_i \left(\frac{\Sigma_R}{\rho}\right)_i \quad (4)$$

where $(\Sigma_R/\rho)_i$ is the mass removal cross-section from the i -th element (cm^2/g), in which the atomic weight function W_i is partial density (g/cm^3) or density of component i in the compound, and ρ is material or compound density (g/cm^3).

The partial density W_i is given by [38]:

$$W_i = x_i \rho \quad (5)$$

where x_i is the weight fraction of i -th constituent in the material, A is an atomic weight and Z is an atomic number.

TABLE 1. Properties of shielding material

Material	Density (g/cm^3)	Composition (atomic fraction)
Aluminium, Al	2.7	1.00
Iron, Fe	7.8	1.00
Concrete [4]	2.3	
^1H		0.023
^{12}C		0.019
^{16}O		0.530
^{27}Al		0.034
^{28}Si		0.337
^{40}Ca		0.044
^{56}Fe		0.014
Borated Polyethylene (BPE) [42]	0.97	
^1H		0.644
^{12}C		0.322
^{16}O		0.022
^{10}B		0.003
^{11}B		0.011

Neutron Dose Reduction factor (RF)

The neutron dose reduction factor (RF) is one of the parameters used to determine the shielding neutron efficiency [43], [44]. RF is the ratio of the ambient dose equivalent at the point of interest with shielding [$H^*(10)_{shield}$] to that without any shielding [$H^*(10)_{no-shield}$]. The equation for calculating the RF is as follows:

$$RF = \left[\frac{H^*(10)_{shield}}{H^*(10)_{no-shield}} \right] \quad (6)$$

RESULT AND DISCUSSION

The Monte Carlo calculation is conducted with a low uncertainty error of less than 5% [35] for most materials and thickness ranges. FIGURE 2 presents the neutron and photon flux on various shielding materials from the PHITS simulation results with a shielding thickness of 105 cm (Z-axis). At the same time, FIGURE 3 shows the neutron energy spectrum in various materials with different thicknesses.

FIGURE 2 shows that Fe outperforms Al, concrete, and BPE at 105 cm depth for blocking fast neutrons of 200 MeV by reducing neutron flux up to 98%. The phenomenon is created by an inelastic scattering interaction between a fast neutron and a high Z material (iron), followed by a low neutron energy level and photon emission. Meanwhile, concrete and aluminum require more than 1.5 times the thickness to reduce the neutron flux with about the same presentation. Furthermore, BPE requires the most considerable thickness, twice as thick as iron.

Compared to a prior work in which Zuo Y et al. [24] did an optimization simulation on neutron shielding from a 14 MeV neutron source, iron demonstrated greater shielding effectiveness than polyethylene materials. Jin-Long Wang et al. [45] also observed the iron configuration on the shielding design for secondary neutrons at the synchrotron-based proton therapy (PT) facility with the injection proton energy of 3.5 MeV has a smaller thickness than the concrete. Consequently, this research verifies previous findings that iron has excellent shielding capabilities for fast neutrons, not only for 14 meV neutron energy distribution and high proton energy distribution but also for 200 MeV neutron energy.

FIGURE 3 further shows that Fe shielding considerably reduces the high-energy neutron spectrum. However, iron is transparent to low energy neutrons around 0.2–0.3 MeV which have the most increased flux along the depth. On the other hand, Al is effective for attenuating resonance and intermediate neutrons with energy less than 1 keV. Most fast and high neutrons penetrate the Al shielding. Meanwhile, concrete can attenuate and absorb a high-energy neutron of 200 MeV but needs thick shielding. Then BPE shows an effective shielding performance for low-energy (thermal) neutrons.

The absorption cross-section significantly affects the neutron energy below 1 eV; therefore, polyethylene material is the best option for low neutron shielding material [12,17,24]. However, there are better choices than polyethylene for fast neutrons. FIGURE 2 shows that most fast and high-energy neutrons penetrate the BPE material. BPE most efficiently attenuates neutron energy up to 1 MeV (FIGURE 3) through elastic scattering reactions. However, BPE is inadequate for attenuating high-energy neutrons of 200 MeV.

Materials containing boron are potentially used as neutron shielding. This material is often enriched with boron-10 isotopes relative to other isotopes to increase the absorber capability of neutrons. Stone et al. revealed that the characteristics of the BPE material show that BPE is a good absorber in a transmission geometry (the shielding position forms a θ – 2θ angle from the part of the neutron source). However, this study shows that BPE should not be used in direct neutron beam vicinity because the significant incoherence of hydrogen nuclear cross-section causes high scattering intensity [10].

The study's findings contradict prior research by Stone et al. [10], in which BPE materials were directly exposed to neutron radiation. FIGURE 2 shows that most neutrons pass through the BPE material, with only a tiny number attenuated or absorbed. As a result, a thick BPE material of 200 cm or greater is required to moderate and absorb fast neutrons with an energy of 200 MeV. This study concludes that BPE should not be used in the region of a direct neutron beam because the large incoherence of the hydrogen nuclear cross-section creates a high scattering intensity.

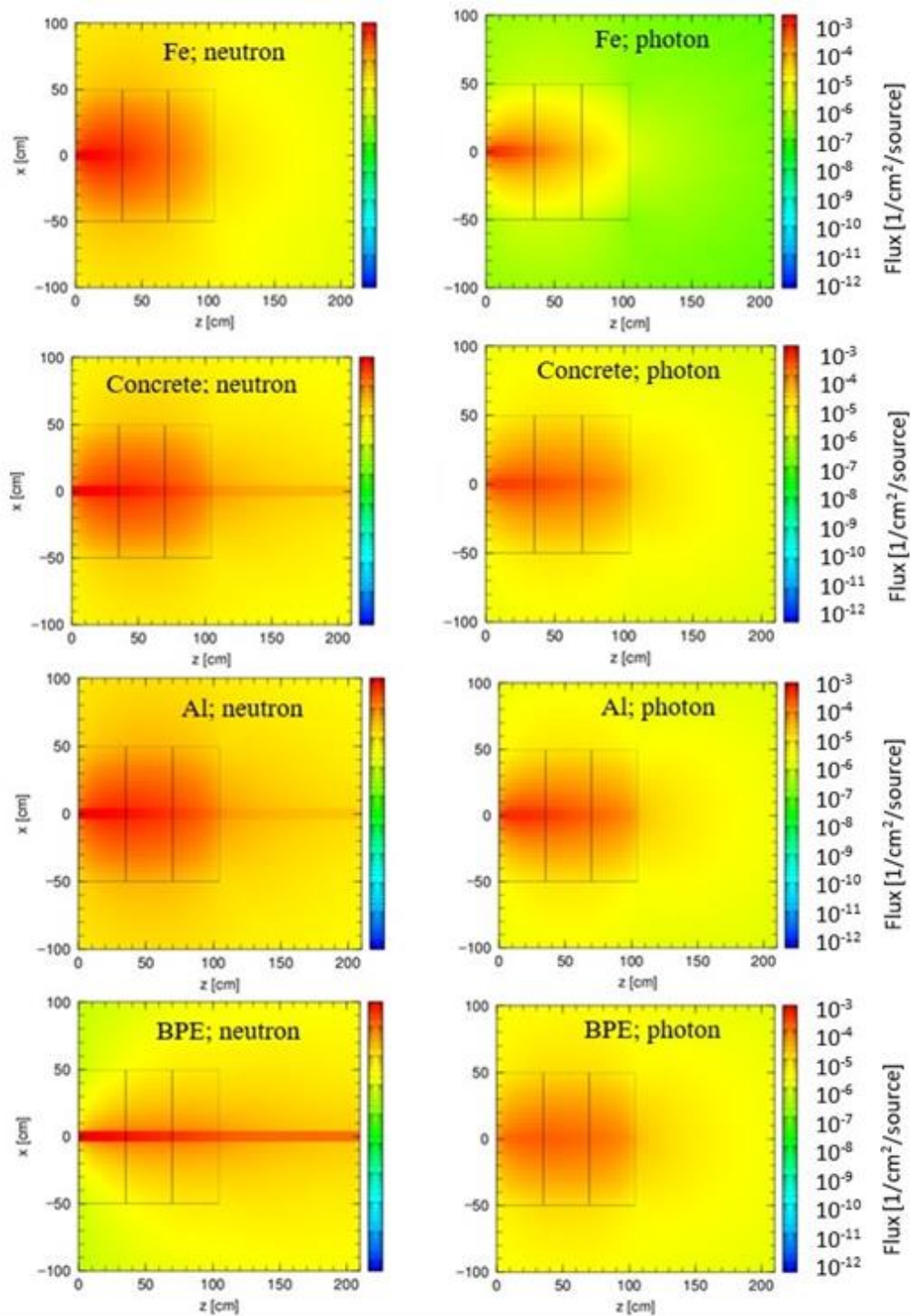


FIGURE 2. Two-dimensional distributions of neutron and photon track length.

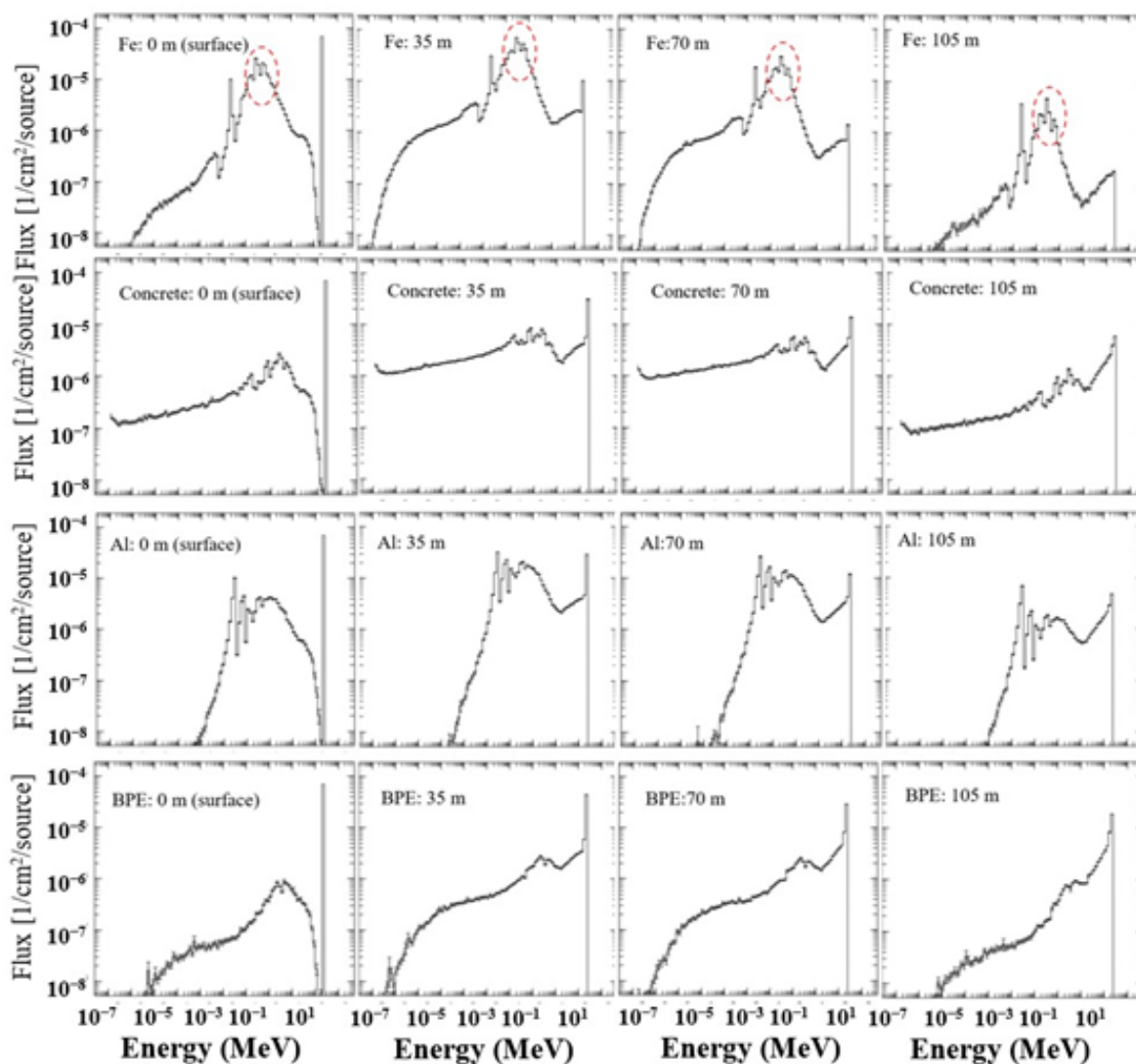


FIGURE 3. Neutron spectrum energy in various materials.

Photons are one of the secondary radiations from the interaction of neutrons with the matter. The selection of shielding considerations for photons depends on the material density. This study agrees with the above theory with adequate materials for photon radiation, namely $\text{Fe} > \text{Al} > \text{concrete} > \text{BPE}$.

An integrated fluence profile versus shielding thickness on various materials (FIGURE 4) shows a good agreement with the result from the experiment and calculations conducted by Eunji Lee et al. [1]. The absolute value of neutron fluence decreases with increasing material thickness. The figure reveals that the effective shielding material for a 200 MeV neutron source is $\text{Fe} > \text{concrete} > \text{Al} > \text{BPE}$.

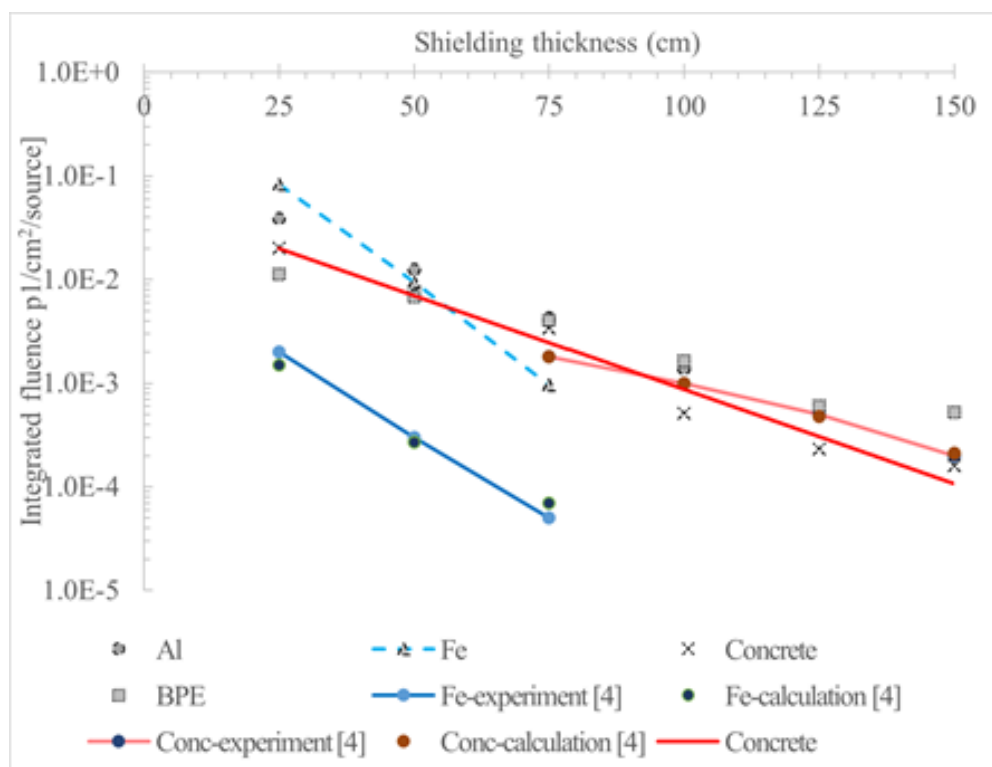


FIGURE 4. Attenuation profile for neutron 200 and 24 MeV [4] in shielding material depth.

Removal cross-section for fast neutron

TABLE 2 shows the calculation of the neutron removal cross-section using the partial density method through EQUATION (5). The removal cross-section value for each element is taken from Elmahroug Y et al. [38], Kaplan [39] and the NBS handbook [46].

TABLE 2 shows that iron has the highest value of the removal cross-section of 0.1560. Meanwhile, the following order is BPE with a removal cross-section value of 0.1132, and the remaining media are Al (0.0813) and concrete (0.0783). Thus, the removal cross-section is dependent on the element composition and density. The hydrogen element has the highest mass removal cross-section of $0.6020 \text{ cm}^2/\text{g}$ because the hydrogen nucleus mass is nearly close to the neutron. Therefore, neutrons and hydrogen have an excellent probability of interaction via elastic scattering. However, the partial density of hydrogen in BPE and concrete is only 0.120 and 0.025, respectively, resulting in the removal cross-section remaining below the iron value. Thus, the calculated Σ_R in TABLE 2 concludes that iron is the best material for attenuating fast neutrons with 200 MeV energy.

TABLE 2. Fast neutron removal cross-section data for iron, aluminum, concrete, and BPE

Element	Weight fraction, x_i	Partial density, W_i (g/cm ³)	Element mass removal cross-section, Σ_R/ρ_i (cm ² /g)	Σ_R (cm ⁻¹)
Fe	1	7.8	0.02	0.1560
Al	1	2.7	0.0301	0.0813
Concrete				
¹ H	0.023	0.05	0.6020	0.0318
¹² C	0.019	0.04	0.0500	0.0022
¹⁶ O	0.530	1.22	0.0410	0.0500
²⁷ Al	0.034	0.08	0.0301	0.0024
²⁸ Si	0.337	0.78	0.0295	0.0229
⁴⁰ Ca	0.044	0.10	0.0240	0.0024
⁵⁶ Fe	0.014	0.03	0.0200	0.0006
		2.30		0.0783
BPE				
¹ H	0.124	0.120	0.6020	0.0723
¹² C	0.599	0.581	0.0500	0.0290
¹⁶ O	0.229	0.222	0.0410	0.0091
¹⁰ B	0.010	0.010	0.0600	0.0006
¹¹ B	0.039	0.037	0.0570	0.0021
		0.97		0.1132

Effective dose and Ambient dose H*(10) equivalent analysis

Comparisons of the distribution profiles of the effective dose of neutron and photon radiation for Fe, Concrete, Al, and BPE materials at various depths are shown in FIGURE 5 in the one-dimensional view. The effective dose of neutron and photon radiation distribution decreases with the increasing depth of shielding material; however, photon only provides a marginal portion. The interesting point is the neutron depth dose profile in iron material, where the effective dose sharply rises at shallow depths and then exponentially decreases with increasing material depth. The highest build-up region is also observed. This build-up is due to the inelastic scattering interaction between neutrons and the iron atomic nucleus, which excites the atomic nucleus after the reaction. The atomic nucleus returns to the ground-level state by emitting photons [47]. The probability of inelastic scattering is high when the neutrons collide with dense material or heavy atomic nuclei. Meanwhile, aluminum and concrete show almost the same dose profile in the shielding material depth. For BPE, the effective neutron dose behind the material remains high, which indicates the escape of numerous neutrons from the BPE shielding material.

The following parameter used to analyze shielding material effectiveness for a neutron energy source of 200 MeV is the ambient dose H*(10) equivalent at the point of interest behind the material provided in TABLE 3. The lowest ambient dose H*(10) equivalent is 7.106×10^{-3} pSv for iron, and the highest is 1.806×10^{-2} pSv for Al. Concrete and BPE have similar ambient doses H*(10) equivalent to 1.496×10^{-2} and 1.502×10^{-2} pSv, respectively.

TABLE 3. Ambient dose $H^*(10)$ equivalent for 200 MeV neutron source

Material	$H^*(10)$ behind 105 cm thickness, pSv
Fe	7.106E-03
Al	1.806E-02
Concrete	1.496E-02
BPE	1.502E-02

Reduction factor (RF)

TABLE 4 calculates the neutron dose RF or shielding factor of material iron, aluminum, concrete, and BPE against 200 MeV mono-energetic neutron radiation through 105 cm thickness. The table reveals that the lowest RF is 0.39 when radiation hits the shielding iron. Meanwhile, aluminum has the highest RF value at 0.99, indicating that aluminum material's effectiveness is deficient against fast neutron radiation. Concrete and BPE have comparable RF figures of 0.82 and 0.83, respectively. TABLE 4 also compares previous studies' RF values for iron and concrete materials. The RF values in the current study agree with the literature. Thus, this RF analysis can conclude that iron is adequate as a shielding material for a fast neutron energy of 200 MeV, followed by concrete, BPE, and aluminum.

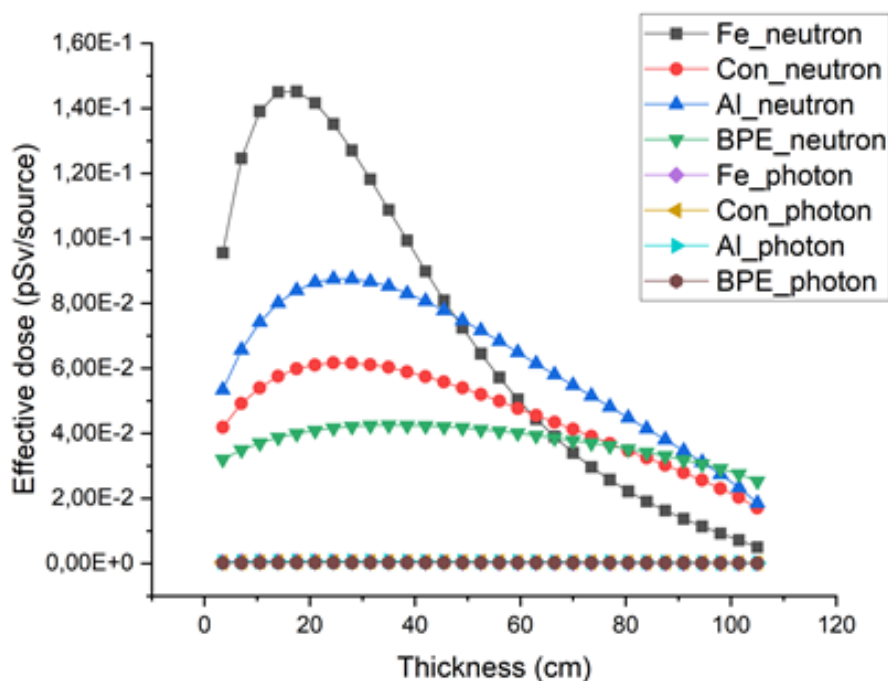
**FIGURE 5.** Effective dose profile in depth from neutron source 200 MeV for various materials

TABLE 4. Reduction factor (RF) or shielding factor for iron, concrete, aluminum, and BPE

Material	$H^*(10)_{\text{shield}}$, pSv	$H^*(10)_{\text{no-shield}}$, pSv	RF present work	RF Ref [44]	RF Ref [48]
Fe	7.106E-03		0.39	0.23–0.34	-
Al	1.806E-02	1.82E-02	0.99	-	-
Concrete	1.496E-02		0.82	-	0.80–0.85
BPE	1.502E-02		0.83	-	-

CONCLUSION

In this analysis, detailed calculations and simulations by the Monte Carlo code of PHITS 3.27 have been conducted to measure the effectiveness of the shielding material against fast neutrons with an energy of 200 MeV. Fluxes of neutrons and photons, integrated fluence, removal cross-section, effective dose, ambient dose $H^*(10)$ equivalent, and RF were calculated for various materials comprising iron, aluminum, concrete, and BPE. The results show that iron is better than concrete, Al, and BPE in blocking fast neutrons with a thickness of 105 cm from visualization of neutron and photon track length. PHITS simulation results show that most neutron radiation penetrates the concrete, Al, and BPE, thus requiring a considerable thickness of shielding materials. An integrated fluence profile confirms that the absolute value of neutron fluence decreases with increasing material thickness. The profile shows a good agreement through the experimental data and calculations from the previous study.

The fast neutron removal cross-section (Σ_R) calculation by a partial density approach shows that iron has the highest Σ_R value while concrete has the lowest Σ_R . By contrast, BPE has a relatively high Σ_R value because it contains a significant fraction of hydrogen atoms. The profile of effective dose amongst shielding depth provided a different characteristic of dose distribution based on neutron interaction within the material. Iron has a vast build-up region in a shallow depth, and then the dose exponentially decreases to the lowest value compared with other materials. The phenomena are caused by inelastic scattering interaction between neutron and high Z material (iron), followed by a low neutron energy level and photon emission.

ACKNOWLEDGEMENT

The authors thank the Malaysian government for financially supporting this research through the Malaysia International Scholarship program and Indonesia National Research and Innovation Agency (BRIN).

REFERENCES

- [1] E. Lee *et al.*, "Energy spectra of neutrons penetrating concrete and steel shielding blocks from 24 GeV/c protons incident on thick copper target," *Nucl. Instruments Methods Phys. Res. Sect. A Accel. Spectrometers, Detect. Assoc. Equipment*, vol. 998, p. 165189, 2021, doi: 10.1016/j.nima.2021.165189.

- [2] H. Paganetti, "Proton Therapy Physics," *Second Edition. Series in Medical Physics and Biomedical Engineering*, Boca Raton, New York: CRC Press, Taylor & Francis Group, 2019.
- [3] J. Y. J. Wei, "Neutrons in Proton Therapy: Quantifying the spatial and angular distribution of lethal neutrons for treatment planning," National University of Singapore, 2019.
- [4] G. F. Garcia-Fernandez *et al.*, "Neutron dosimetry and shielding verification in commissioning of Compact Proton Therapy Centers (CPTC) using MCNP6.2 Monte Carlo code," *Applied Radiation and Isotopes*, vol. 169, p. 109279, 2021, doi: 10.1016/j.apradiso.2020.109279.
- [5] W. D. Newhauser and R. Zhang, "The physics of proton therapy," *Physics in Medicine & Biology*, vol. 60, no. 8, pp. R155-R209, 2015, doi: 10.1088/0031-9155/60/8/R155.
- [6] E. Mansouri *et al.*, "A review on neutron shielding performance of nanocomposite materials," *International Journal of Radiation Research*, vol. 18, no. 4, pp. 611-622, 2020, doi: 10.18869/acadpub.ijrr.18.4.611.
- [7] PTCOG, "Practice Considerations for Proton Beam Radiation Therapy of Uveal Melanoma During the Coronavirus Disease Pandemic," Particle Therapy Co-operative Group, 2020, [Online], Available: <https://www.ptcog.ch/>.
- [8] F. Aliyah, S. G. Pinasti and A. A. Rahman, "Proton therapy facilities: an overview of the development in recent years," *IOP Conference Series: Earth and Environmental Science*, vol. 927, no. 1, p. 012042, 2021, doi: 10.1088/1755-1315/927/1/012042.
- [9] J. E. Tepper, R. L. Foote and J. M. Michalski, "Clinical Radiation Oncology," *Elsevier Health Sciences*, Philadelphia: Elsevier, 2021.
- [10] M. B. Stone *et al.*, "Characterization of shielding materials used in neutron scattering instrumentation," *Nuclear Instruments and Methods in Physics Research Section A: Accelerators, Spectrometers, Detectors and Associated Equipment*, vol. 946, p. 162708, 2019, doi: 10.1016/j.nima.2019.162708.
- [11] T. Nunomiya *et al.*, "Measurements of neutron attenuation through iron and concrete at ISIS," *Journal of Nuclear Science and Technology*, vol. 37, no. 1, pp. 158-161, 2000, doi: 10.1080/00223131.2000.10874866.
- [12] M. Fragopoulou and M. Zamani, "Phenomenological calculations of shielding spallation neutron sources," *Nuclear Instruments and Methods in Physics Research Section A: Accelerators, Spectrometers, Detectors and Associated Equipment*, vol. 714, pp. 24-30, 2013, doi: 10.1016/j.nima.2013.02.023.
- [13] T. Piotrowski, "Neutron shielding evaluation of concretes and mortars: A review," *Construction and Building Materials*, vol. 277, p. 122238, 2021, doi: 10.1016/j.conbuildmat.2020.122238.
- [14] S. Hashimoto *et al.*, "PHITS Simulation of Quasi-Monoenergetic Neutron Sources from ${}^7\text{Li}(p,n)$ Reactions," *Energy Procedia*, vol. 71, pp. 191-196, 2015, doi: 10.1016/j.egypro.2014.11.869.
- [15] T. Sato *et al.*, "Features of Particle and Heavy Ion Transport code System (PHITS) version 3.02," *Journal of Nuclear Science and Technology*, vol. 55, no. 6, pp. 684-690, 2018, doi: 10.1080/00223131.2017.1419890.

- [16] J. W. Shin *et al.*, “GEANT4 and PHITS simulations of the shielding of neutrons from the ^{252}Cf source,” *Journal of the Korean Physical Society*, vol. 65, no. 5, pp. 591-598, 2014, doi: 10.3938/jkps.65.591.
- [17] S. F. Olukotun *et al.*, “The effect of incorporated recycled low density polyethylene (LDPE) on the fast neutron shielding behaviour (FNSB) of clay matrix using MCNP and PHITS Monte Carlo codes,” *Radiation Physics and Chemistry*, vol. 182, p. 109351, 2021, doi: 10.1016/j.radphyschem.2021.109351.
- [18] X. Zhang *et al.*, “Benchmarking GEANT4 and PHITS for 14.8-MeV neutron transport in polyethylene and graphite materials,” *Fusion Engineering and Design*, vol. 170, p. 112720, 2021, doi: 10.1016/j.fusengdes.2021.112720.
- [19] Y. Iwamoto *et al.*, “Measurements and Monte Carlo calculations of forward-angle secondary-neutron-production cross-sections for 137 and 200 MeV proton-induced reactions in carbon,” *Nuclear Instruments and Methods in Physics Research Section A: Accelerators, Spectrometers, Detectors and Associated Equipment*, vol. 690, pp. 1-16, 2012, doi: 10.1016/j.nima.2012.06.038.
- [20] H. Iwamoto and S. I. Meigo, “Validation of PHITS Spallation Models from the Perspective of the Shielding Design of Transmutation Experimental Facility,” *EPJ Web of Conferences*, vol. 153, pp. 1-9, 2017, doi: 10.1051/epjconf/201715301016.
- [21] F. Cadini *et al.*, “Neutron shielding for a new projected proton therapy facility: A Geant4 simulation study,” *Physica Medica*, vol. 32, no. 12, pp. 1862-1871, 2016, doi: 10.1016/j.ejmp.2016.12.003.
- [22] D. R. McAlister, “Neutron Shielding Materials,” University Lane Lisle USA, 2016.
- [23] A. Glovebox, S. Annual and C. Dees, “Neutron Radiation Shielding Strategies for Glovebox Applications,” Idaho National Lab, United States, 2017.
- [24] Y. Zuo *et al.*, “Monte Carlo optimization simulation of neutron shielding performance of iron/polyethylene combined structure,” *MATEC Web of Conferences*, vol. 189, p. 02001, 2018, doi: 10.1051/mateconf/201818902001.
- [25] G. Hu *et al.*, “New shielding material development for compact accelerator-driven neutron source,” *AIP Advances*, vol. 7, no. 4, p. 045213, 2017, doi: 10.1063/1.4982241.
- [26] F. Tovesson and T. S. Hill, “Neutron induced fission cross section of ^{237}Np from 100 keV to 200 MeV,” *Physical Review C*, vol. 75, no. 3, p. 34610, 2007, doi: 10.1103/PhysRevC.75.034610.
- [27] T. Koi *et al.*, “Attenuation of neutrons in the atmosphere and a thick carbon target,” *Nuclear Instruments and Methods in Physics Research Section A: Accelerators, Spectrometers, Detectors and Associated Equipment*, vol. 469, no. 1, pp. 63-69, 2001, doi: 10.1016/S0168-9002(01)00289-3.
- [28] V. P. Singh and N. M. Badiger, “Gamma ray and neutron shielding properties of some alloy materials,” *Annals of Nuclear Energy*, vol. 64, pp. 301-310, 2014, doi: 10.1016/j.anucene.2013.10.003.
- [29] S. Agosteo *et al.*, “Shielding data for 100-250 MeV proton accelerators: Double differential neutron distributions and attenuation in concrete,” *Nuclear Instruments and Methods in Physics Research Section B: Beam Interactions with Materials and Atoms*, vol. 265, no. 2, pp. 581-598, 2007, doi: 10.1016/j.nimb.2007.09.046.

- [30] S. Agosteo, M. Magistris, A. Mereghetti, M. Silari, and Z. Zajacova, "Shielding data for 100-250 MeV proton accelerators: Attenuation of secondary radiation in thick iron and concrete/iron shields," *Nuclear Instruments and Methods in Physics Research Section B: Beam Interactions with Materials and Atoms*, vol. 266, no. 15, pp. 3406-3416, 2008, doi: 10.1016/j.nimb.2008.05.002.
- [31] G. Zhang, "Monte Carlo Simulation of Mixed Neutron-Gamma Radiation Fields and Dosimetry Devices," pp. 1-150, 2011.
- [32] J. S. Alzahrani *et al.*, "Simulating the radiation shielding properties of TeO₂-Na₂O-TiO glass system using PHITS Monte Carlo code," *Computational Materials Science*, vol. 196, p. 110566, 2021, doi: 10.1016/j.commatsci.2021.110566.
- [33] A. F. Bielajew, "Fundamentals of the Monte Carlo method for neutral and charged particle transport," The University of Michigan, 2020.
- [34] T. R. Ayodele, "Analysis of Monte Carlo Simulation Sampling Generator- Connected Power System," *Journal English Science Technology*, vol. 11, no. 4, pp. 563-583, 2016.
- [35] B. Harding, C. Tremblay and D. Cousineau, "Standard errors: A review and evaluation of standard error estimators using Monte Carlo simulations," *The Quantitative Methods for Psychology*, vol. 10, no. 2, pp. 107-123, 2014, doi: 10.20982/tqmp.10.2.p107.
- [36] E. P. Blizard *et al.*, "Atomic energy commission, Division of technical information," Reactor handbook, London: Interscience, 1962.
- [37] J. J. Duderstadt and L. J. Hamilton, "Nuclear Reactor Analysis." John Wiley & Sons, New York, USA, 1976.
- [38] Y. Elmahroug, B. Tellili and C. Souga, "Determination of shielding parameters for different types of resins," *Annals of Nuclear Energy*, vol. 63, pp. 619-623, 2014, doi: 10.1016/j.anucene.2013.09.007.
- [39] M. F. Kaplan, "Concrete radiation shielding: nuclear physics, concrete properties, design and construction," Harlow; New York: Longman Scientific & Technical ; Wiley, 1989.
- [40] S. Glasstone, "Nuclear reactor engineering," New York, NY: Chapman & Hall, 1994.
- [41] W. M. Stacey, "Nuclear reactor physics," John Wiley & Sons, 2018.
- [42] B. Ma *et al.*, "Shielding design of a target station and radiation dose level investigation of proton linac for a compact accelerator-driven neutron source applied at industrial sites," *Applied Radiation and Isotopes*, vol. 137, no. 28, pp. 129-138, 2018, doi: 10.1016/j.apradiso.2018.03.015.
- [43] H. Yoshida-Ohuchi *et al.*, "Reduction factors for wooden houses due to external γ -radiation based on in situ measurements after the Fukushima nuclear accident," *Scientific Reports*, vol. 4, no. 1, p. 7541, 2014, doi: 10.1038/srep07541.
- [44] H. Yoshida-Ohuchi, N. Matsuda and K. Saito, "Review of reduction factors by buildings for gamma radiation from radiocaesium deposited on the ground due to fallout," *Journal of environmental radioactivity*, vol. 210, p. 105810, 2019, doi: 10.1016/j.jenvrad.2018.09.008.
- [45] J. L. Wang *et al.*, "Radiation shielding design of a compact single-room proton therapy based on synchrotron," *Nuclear Science and Techniques*, vol. 31, no. 1, pp. 1-12, 2020, doi: 10.1007/s41365-019-0712-1.

- [46] S. Weeks and A. Astin, "Protection Against Neutron Radiation Up to 30 Million Electron Volts," Washington: National Bureau of Standards, 1957.
- [47] A. F. Mkhairber and S. K. Dawood, "Calculation of Shielding Parameters of Fast Neutrons for Some Composite Materials," *Al-Mustansiriyah Journal of Science*, vol. 30, no. 1, pp. 210-215, 2019, doi: 10.23851/mjs.v30i1.520.
- [48] Wu, Hwai-Chung and C. D. Eamon, "Strengthening of concrete structures using fiber reinforced polymers (FRP): design, construction and practical applications," 2017.